# Generation of multiple vortex-cones by direct-phase modulation of annular aperture array

Seong-Woo Cho,[1] Hwi Kim,[2,*] Joonku Hahn,[3] and Byoungho Lee[1]

[1]National Creative Research Center for Active Plasmonics Application Systems, Inter-University Semiconductor Research Center and School of Electrical Engineering, Seoul National University, Gwanakgu Gwanakro 1, Seoul 151-744, South Korea

[2]Department of Electronics and Information Engineering, College of Science and Technology, Korea University, Sejong Campus, Sejong-ro 2511, Sejong 339-700, South Korea

[3]School of Electronics Engineering, Kyungpook National University, Buk-Gu Sankyuk-Dong, Daegu 702-701, South Korea

*Corresponding author: hwikim@korea.ac.kr

Received 22 June 2012; revised 31 August 2012; accepted 3 September 2012; posted 21 September 2012 (Doc. ID 171073); published 16 October 2012

The generation of multiple vortex cones using an annular aperture array and a spatial light modulator (SLM) is studied. The direct downscale imaging of an SLM on the surface of an annular aperture enables the direct-phase modulation of the annular aperture. It is experimentally demonstrated that the direct-phase modulation of an annular aperture array can control both the topological charge and the horizontal positions of multiple vortex cones simultaneously. 

*OCIS codes:* 140.3300, 110.0110, 070.6120.

## 1. Introduction

Special types of optical beams, such as Bessel beams [1–4], Airy beams [5,6], and plasmonic mediated microbeams [7,8] have been actively researched for practical applications as well as fundamental research. Among them, optical beams with phase singularity generated by a spiral phase plate, referred to as vortex beams, attract lots of research interest recently [1–4,9,10]. Practical applications, such as optical tweezers, optical trapping, and optical imaging adopt the unique advantages of using optical vortex beams [9–13]. For some biological sensing and lithography applications, the beam formation in the range from 1 to 10 μm from the substrate and its dynamic control are desired. Recently, the beam array formation in the midfield region using a planar annular aperture array was studied for sensing applications [14]. From the same reason, the vortex beam formation in the midfield region is also of interest for the similar applications.

In general, an optical plane wave (assumed to be under normal incidence) that passes through a circular aperture with a spiral phase plate is transformed to a slightly diverging vortex beam in the free space. The vortex beam has a phase singularity at the center of the beam. As a result, a dark region appears at the center of the beam. From a three-dimensional viewpoint, as the phase singularity propagates toward free space, a three-dimensional dark shadow region is formed along the beam profile. This is referred to as a vortex cone.

In this paper, the generation and dynamic control of tiny multiple vortex cones using a microscale annular aperture array and a phase-type spatial light modulator (SLM) is studied. The SLM is the active diffractive optic device for dynamic optical wavefront modulation [15–19], and amplitude-type and phase-type SLMs are commercialized. To synthesize the vortex beam, the spiral phase modulation of optical wave is necessary. Considering the practical

1559-128X/12/307295-08$15.00/0

condition of vortex field formation using the pixelated SLM, we devise an effective way of generating vortex patterns that the phase-type SLM is directly downscale-imaged onto the surface of the annular aperture array and modulates the circumference phase profile of the annular aperture array. As a result, a microscale annular aperture phase-type SLM is obtained. It is experimentally demonstrated that dynamic and simultaneous control of the topological charge and positional translation of multiple vortex cones is enabled with the proposed direct-phase modulation technique.

This paper is organized as follows. In Section 2, the optical vortex field formation using a phase-modulated annular aperture is introduced and some optical properties related to finite pixelation of the SLM are discussed. In Section 3, the dynamic manipulation of multiple vortex cones is demonstrated experimentally. In Section 4, concluding remarks are given.

## 2. Optical Vortex Field Generation Using a Phase-Modulated Annular Aperture

Figures 1(a) and 1(b) present the three-dimensional field profiles of vortex beams generated with a circular aperture [20] and an annular aperture with the same diameter and spiral phase profile of the same topological charge, respectively. The optical field on the surface of an annular aperture is given by $A(x,y)\exp(jm\varphi(x,y))$, where $A(x,y)=1$ when $r_i^2 \le x^2+y^2 \le r_o^2$ at $z=0$; $A(x,y)=0$ otherwise, where $r_i$ and $r_o$ are the inner and outer radii of the annular aperture, respectively. The phase modulation is considered to be of the $m$th order, when the phase modulation is $m\varphi$, where $m$ is an integer and $\varphi$ varies from 0 to $2\pi$, $\varphi=\tan^{-1}(y/x)$. As an example, a third-order vortex cone with the linear phase modulation of 0–$6\pi$ along the annular aperture perimeter in the counterclockwise direction is simulated based on the scalar diffraction theory [21]. The field distribution in the free space is calculated by the angular spectrum integral, which takes the form of

$$F(x,y,z)=\int_{-\infty}^{\infty}\int_{-\infty}^{\infty}\tilde{A}(\alpha,\beta)\exp(j2\pi(\alpha x+\beta y+\gamma z))\mathrm{d}\alpha\mathrm{d}\beta, \tag{1a}$$

where $\alpha$ and $\beta$ are the $x$- and $y$-directional spatial frequency components, respectively. The $z$-directional spatial frequency $\gamma$ is $\gamma=\sqrt{(1/\lambda)^2-\alpha^2-\beta^2}$, and $\tilde{A}(\alpha,\beta)$ is the two-dimensional Fourier transform of an annular aperture with spiral phase profile obtained by

$$\tilde{A}(\alpha,\beta)=\int_{-\infty}^{\infty}\int_{-\infty}^{\infty}A(x,y)\exp(jm\varphi(x,y))\times\exp(-j2\pi(\alpha x+\beta y))\mathrm{d}\alpha\mathrm{d}\beta. \tag{1b}$$

In the simulations of Fig. 1, the vortex field generations of the circular aperture with a radius 15 μm, and the annular aperture with an outer radius 15 μm and an inner radius 14 μm, are compared. Each point on the circular slit has a phase of $\exp(i3\varphi)$. The spiral phase profiles for the cases of circular aperture and annular aperture are presented in Figs. 1(a) and 1(b), respectively. As shown in Fig. 1(c), a dark vortex cone wrapped by a bright, cone-shaped caustic surface is formed along the optical axis. Figure 1(d) shows that although the annular aperture filters the incident optical field instead of the circular aperture, as shown in Fig. 1(b), the vortex beam is clearly formed in the free space. The vortex shaping of the circular and annular apertures look similar but transmission efficiency of the incident wave for the annular aperture is obviously lower than that for the circular aperture.

However, in practice, the use of the annular aperture has a necessity for some specific applications. Let us consider an example of formation of the vortex field with the topological charge of 20 in the midfield region. The midfield region is defined in Ref. [14], which is the region important for biosensing and lithography, and it is indicated by the white dashed rectangles near the aperture surface in Figs. 1(c) and 1(d).

The vortex field formations at $z=10$ μm using a conventional pixelated phase-type SLM and the circular and annular apertures are comparatively analyzed. Here, the effect of the finite pixel size of the SLM used to modulate apertures is mainly focused on. In Figs 2(a) and 2(b), the continuous phase profile in the circular aperture with a radius of $r=15$ μm and the resulting vortex field profile measured at the midfield plane $z=10$ μm are shown, respectively. The vortex formation is clear, where the inset shows the detailed double vortex structure inside the main vortex field.

Assuming that the SLM is pixelated with a finite pixel size (1.24 μm × 1.24 μm), we can see in Fig. 2(c) that the central part of the pixelated SLM is not able to provide sufficient pixel resolution for correctly displaying fine spiral phase profile with the topological charge of 20. This undersampling of the phase profile leads to the destruction of the central dark area of the vortex field as presented in Fig. 3(d). In particular, this effect of the pixelation is significant on the formation of higher order vortex fields in the midfield region, since as the higher the topological charge becomes, the finer the resolution of the spiral phase profile around the center should be.

In Fig. 3, the similar simulation results obtained with the annular aperture are presented. It is shown that the annular aperture can also make the vortex field with the topological charge of 20 successfully. The synthesized small vortex field has the same radius as the inner vortex generated by the circular aperture in Fig. 3(b). When the circumference of the annular aperture is pixelated as shown in Fig. 3(c), the degradation in the field distribution outside the vortex dark region is observed, but the dark area of the vortex pattern is still persistent for the pixelation of the phase modulation [Fig 3(d)], which

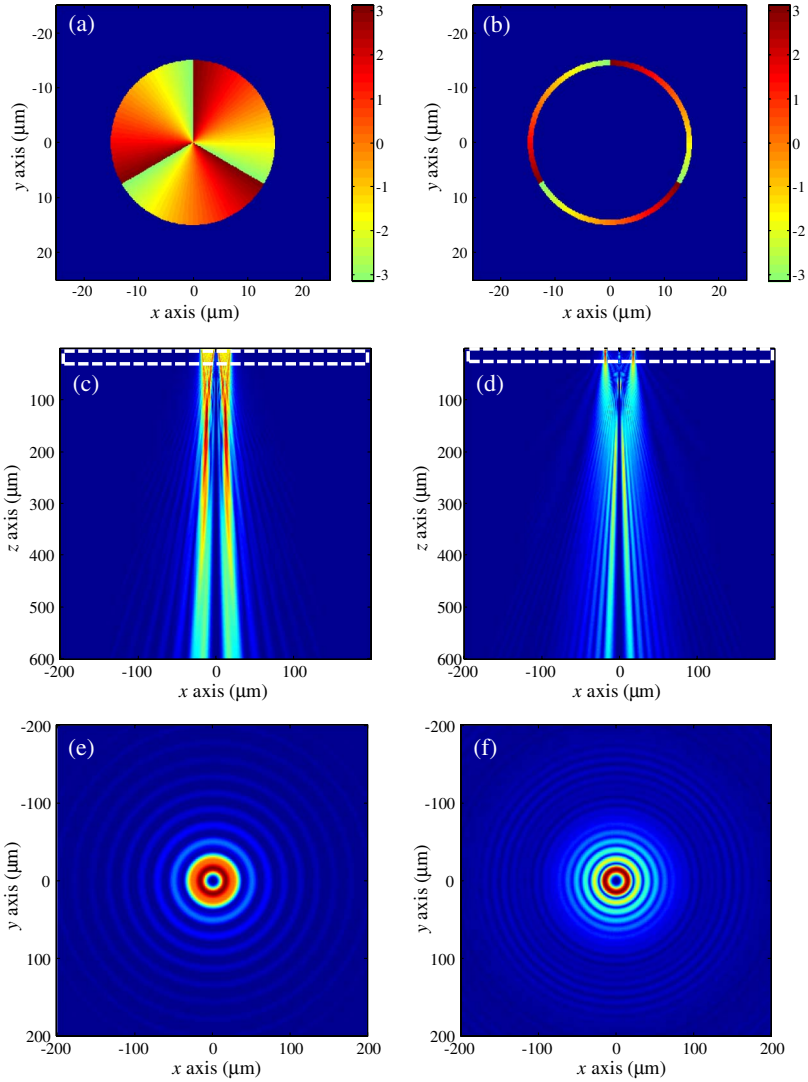


Fig. 1. (Color online) Phase profiles of (a) the circular aperture and (b) the annular aperture are shown, where the phase profiles are given by $\exp(i3\varphi)$, where $\varphi$ as given by $\varphi = \tan^{-1}(y/x)$ varies from 0 to $2\pi$. The $x$-$z$ plane cross-sections of (c) the circular aperture and (d) the annular aperture show a slightly diverging profile of the vortex cone. The $x$-$y$ plane cross-sections ($z = 300$ μm) of (e) the circular aperture and (f) the annular aperture show vortex profiles with bright vortex ring.

is in contrast to the result in Fig. 2(d). The reason for this phenomenon can be understood as the pixelated phase modulation of the annular aperture being approximate but sufficient to give a fine spiral angular momentum to the diffraction field. In the case of the circular aperture, the phase profile around the center is undersampled due to the finite pixel size so the fine vortex field pattern does not appear. This difference between annular aperture and circular aperture is more apparent in the midfield region ($0 \le z \le 100$ μm).

The feasibility of generating the vortex pattern using the direct phase modulation of the annular aperture with the pixelated SLM allows us to create microscale multiple higher-order vortex cones in the midfield region which are narrowly separated. The use of annular aperture rather than circular aperture is more advantageous in the synthesis of close interdistanced multiple vortex patterns. The function of generating higher-order vortices with tens of topological charge, which realize high optical angular momentum in the midfield region, might be meaningful for tweezing applications.

Meanwhile, the transmission efficiency of the annular aperture is simply calculated by the ratio of the annular opened area to the circular aperture area, $(r_o^2 - r_i^2)/r_o^2$. From the above discussion, the minimum inner radius of the annular aperture that is necessary to persist the vortex dark area precisely can be considered as a function of the topological charge and the finite pixel size of the phase modulation. The higher the topological charge assigned, the wider the area around the center that cannot sufficiently represent the spiral phase profile. The incorrectly undersampled area within the outer circle of the outer radius $r_o$ is blocked by the circular mask of the inner

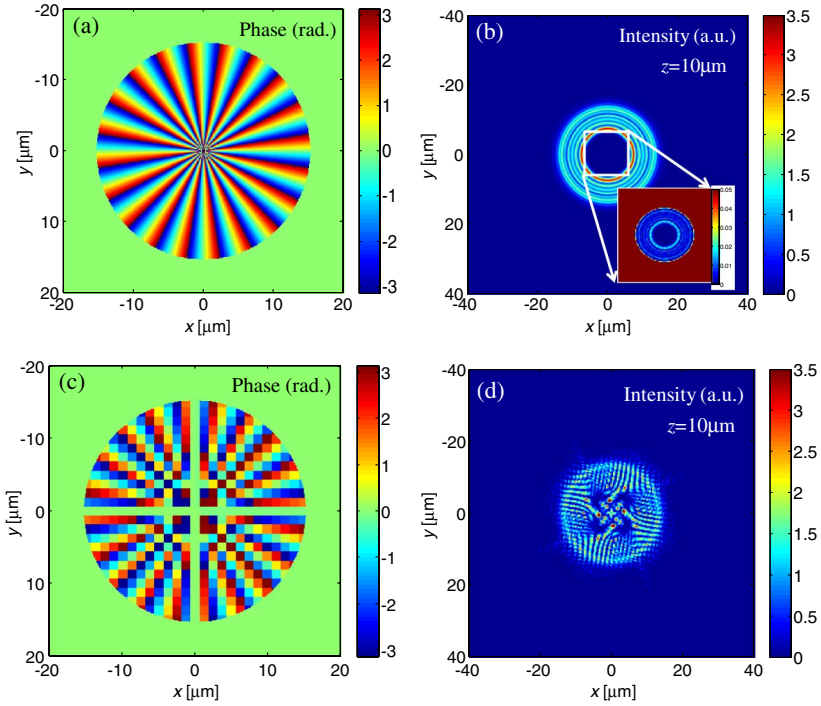


Fig. 2. (Color online) Effect of the pixelated spiral phase modulation of the circular aperture on the formation of midfield vortex field formation: (a) phase profile of the circular aperture with a topological charge of 20 and (b) the resulting optical intensity profile at $z = 10$ μm. (c) The pixelated phase profile with the pixel size 1.24 μm × 1.24 μm and the same topological charge and (d) the resulting optical intensity profile at $z = 10$ μm.

radius $r_i$ of the annular aperture. Therefore, the achievable transmission efficiency is determined by the topological charge of the designed vortex field.

In the following sections, we investigate the experimental dynamic control of multiple vortex patterns by the direct phase modulation of the

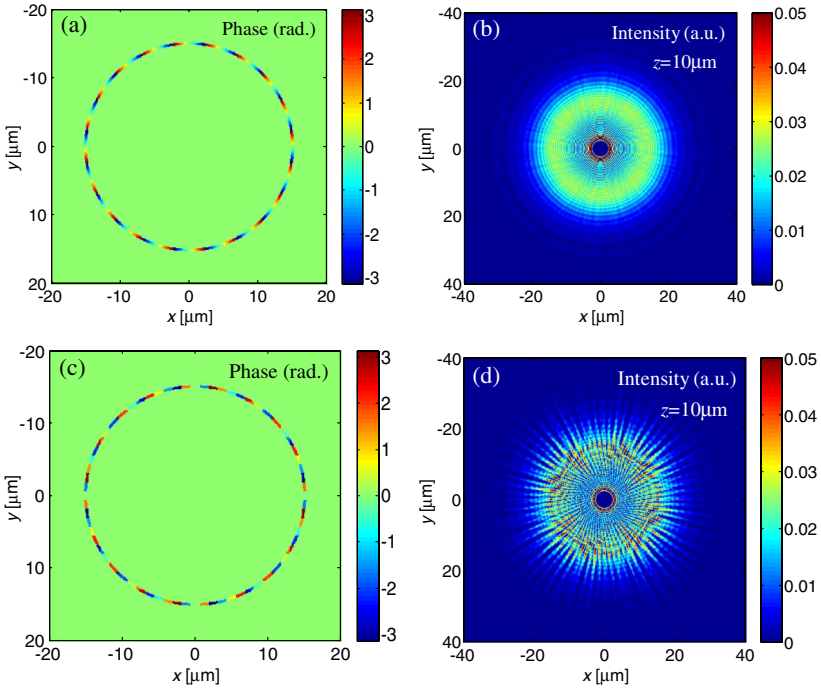


Fig. 3. (Color online) Effect of the pixelated spiral phase modulation of the annular aperture on the formation of midfield vortex field formation: (a) phase profile of the annular aperture with a topological charge of 20 and (b) the resulting optical intensity profile at $z = 10$ μm. (c) The pixelated phase profile with the pixel size 1.24 μm × 1.24 μm and the same topological charge and (d) the resulting optical intensity profile at $z = 10$ μm.

circumference of the annular aperture using the phase-type SLM in the following section.

### 3. Generation and Control of Multiple Vortex Patterns with Direct-Phase Modulation of an Annular Aperture

Before discussing the generation of multiple vortex patterns, we investigate the formation of single vortex pattern with the direct-phase modulation of annular aperture. In Fig. 4, vortex cones synthesized by the annular aperture ($r_i = 14$ μm, $r_o = 15$ μm) with several orders of phase modulation are presented. As shown in Fig. 4, the zeroth-order beam is a Bessel beam with a bright center. The figure shows that the divergence angle of the vortex cone wrapped with a thin vortex caustic surface increases with the order of the phase modulation.

In Figs. 5(a) and 5(b), a scanning electron microscope (SEM) image of the annular ring aperture used in the experiment is presented and the experimental setup for the synthesis and measurement of the vortex cones is schematically illustrated, respectively. To fabricate the sample, silver film 300 nm thick was deposited on a fused silica wafer. An annular aperture with a radius of 30 μm was then inscribed on the silver surface. In the experimental setup, the proposed direct-phase modulation technique through downscale imaging of an SLM on an annular aperture is implemented.

A laser with a wavelength of 660 nm goes through half wave plate (HWP) and a beam expander, and the expanded light propagates to the phase-type SLM (PLUTO of Holoeye). The HWP makes the horizontal polarization state for normal operation of SLM. This SLM changes the phase of the light and supplies the proper phase variation to form the vortex cone at the annular aperture on the silver surface. The complex image of the SLM is scaled down by a convex lens (Lens 1), a concave lens (Lens 2), and an objective lens, and, consequently, a demagnified SLM image appears on the backside of the annular aperture. The obtained demagnification power is 1/72. Accurate alignment is a key requirement. To align the SLM image with the center of the annular aperture, charge-coupled device (CCD) 1 captures the overlapped image of the reflected SLM image from the backside of the annular aperture sample and the annular aperture image itself through a beam splitter. Field images of the vortex cones are captured by CCD 2. In the proposed system, any misalignment between the phase profile and the annular aperture can be readily adjusted by electrically tuning the position of the phase profile image on the SLM because the SLM image and the annular aperture can be monitored *in situ*.

Figure 5(c) shows that the experimental results nearly match the simulation results of Fig. 4. On the surface, as shown in Fig. 5(c), all of the light coming from the aperture has the same circular shape. When moved away from the surface, each cone forms a differently sized circular pattern according to the respective topological charge. Whereas the shape of the zeroth-order beam is a Gaussian beam, the other beams have the shape of a ring of which the center is a dark area. As the beam propagates longer, the dark area size becomes larger and the beam becomes cone-shaped. A higher order cone forms a vortex ring with a larger diameter ring than a lower order cone. As verified in the experimental result, the proposed direct downscale imaging technique of an SLM for the phase modulation of the annular aperture performed successfully in the simultaneous control of the topological charge and the horizontal translation of a vortex cone. This technique can be considered as a type of complex modulation with which both the phase and amplitude are controlled.

By tuning the magnification rate of the optical system, we can control the size of the SLM image on the aperture plane. Thus, it is possible to modulate the phase profile of multiple annular apertures simultaneously using the direct-phase modulation technique. In this section, four closely separated vortex

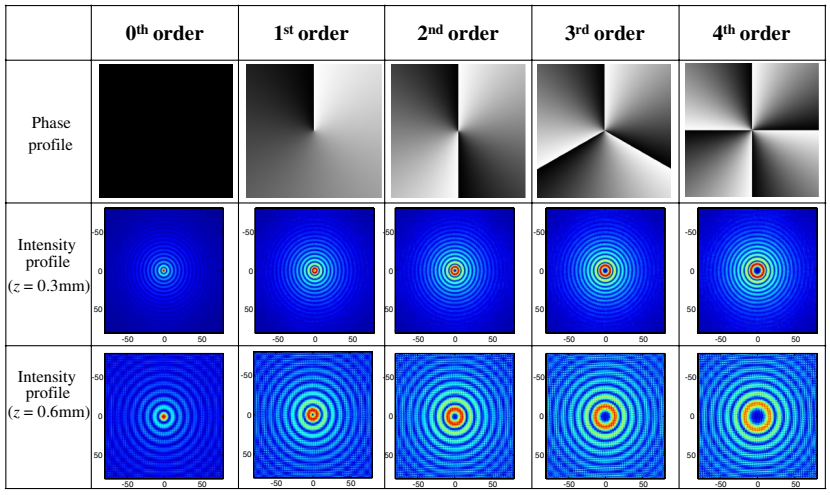


Fig. 4. (Color online) Phase modulation profiles of the zeroth to the fourth topological charges to be displayed on the SLM and the $x$–$y$ cross-sections of the corresponding optical field profiles at $z = 0.3$ mm and 0.6 mm.

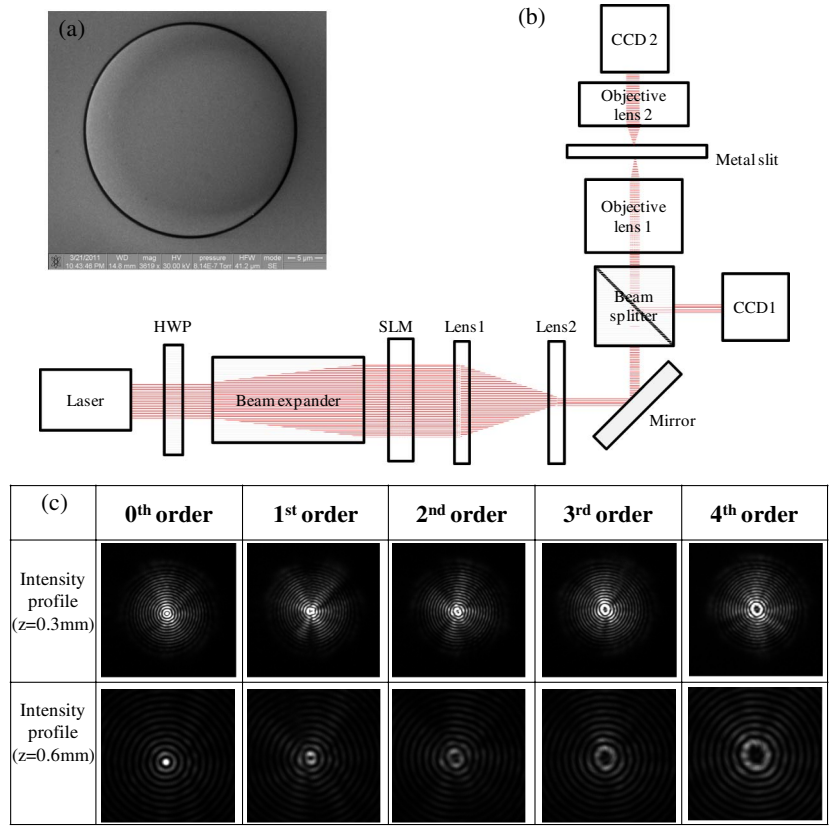


Fig. 5. (Color online) (a) SEM image of the annular aperture inscribed on the silver surface. (b) The overall experimental setup is shown, as are (c) optical intensity profiles experimentally measured at the planes ($z = 0.3$ mm and $z = 0.6$ mm) above the aperture surface.

cones are generated and their topological charges and horizontal translations are controlled with sectional spiral-phase encoding. A phase SLM divided into four quadrants is used, and the four quadrants of the SLM have different instances of phase information with four different topological charges, as shown in Fig. 6(a), which is imposed on the annular aperture array shown in Fig. 6(b), as was inscribed on the silver film.

The experimental setup is identical to that of the single-aperture experiment. The film thickness, aperture radius, and demagnification power are also the same as those in the previous single-aperture experiment. The distance between each aperture is 30 μm. If the number of apertures or the distance between the apertures is increased, the demagnified SLM image may not cover all of the apertures. In such a case, the demagnification power should be decreased. The simulation and experiment results are shown, respectively, in Figs. 6(c) and 6(d). The right upper pattern is the zeroth-order cone, and the left upper cone, the left lower cone, and the right lower cone are the third-order cone, the fifth-order cone, and the fourth-order cone, respectively. Multiple vortex cones can be formed and controlled separately with the phase SLM.

On the other hand, the addition of a blazed linear phase profile to the spiral phase makes the generated vortex cone shift horizontally on a specific

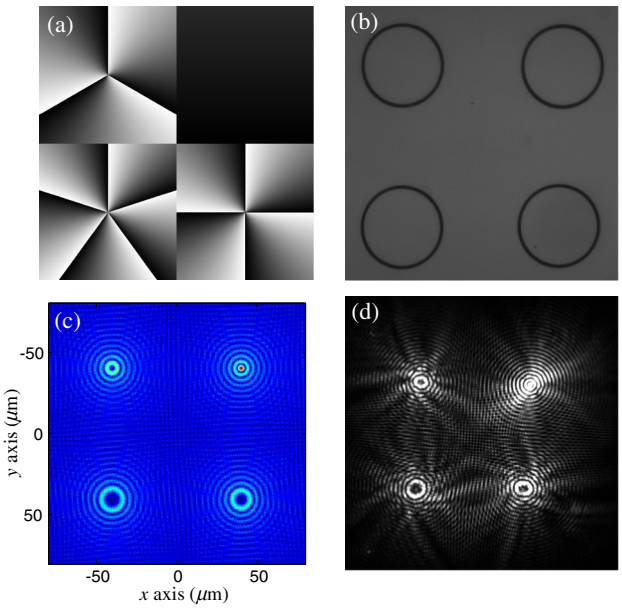


Fig. 6. (Color online) (a) Phase modulation profiles and (b) a CCD image of annular aperture array. (c) Simulation and (d) experimental results of multiple vortex cones. The right upper vortex cone denotes the zeroth-order topological charge (no vortex) and the left upper, left lower, and right lower vortex cones denote the third-order, fifth-order, and fourth-order topological charges, respectively.

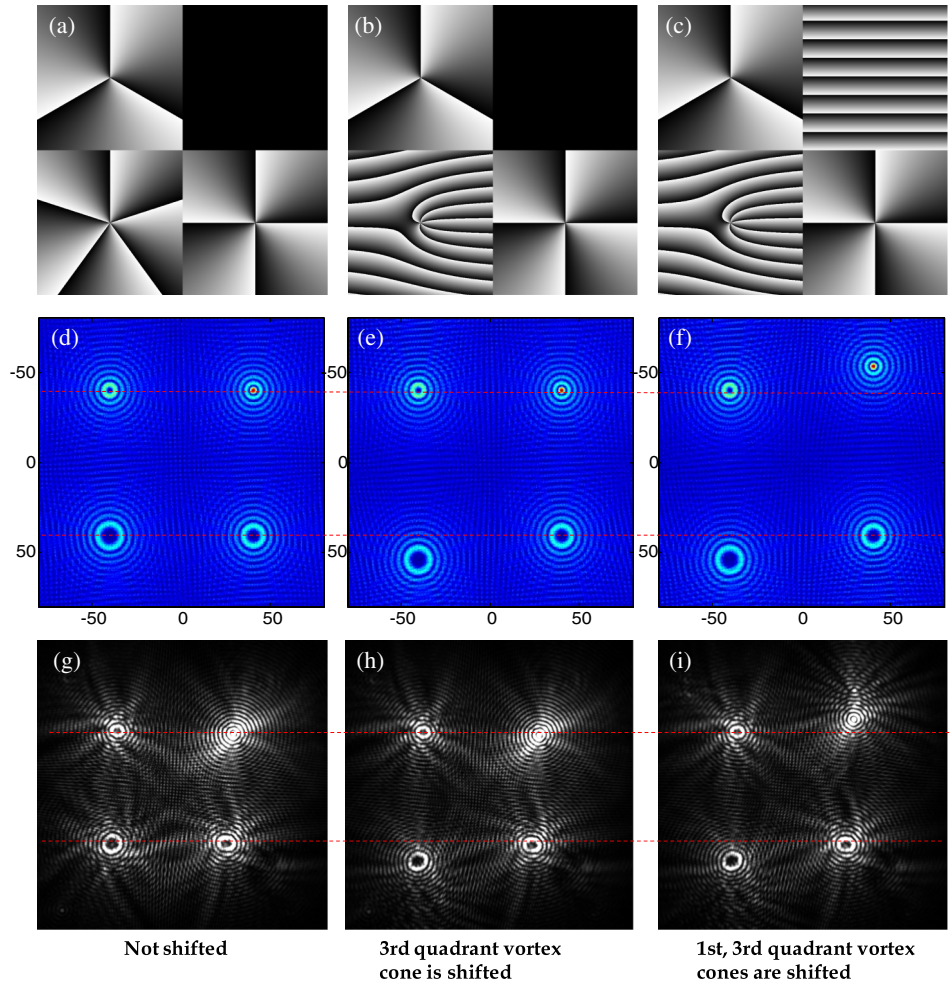


Fig. 7. (Color online) Phase profiles to induce [(a)–(c)] the spatial shifting of the vortex cones, [(d)–(f)] the corresponding simulations, and [(g)–(i)] the experiment results. In this experiment, the vortex cones in the first and third quadrant regions are shifted. The dotted reference lines are drawn for a comparison of the spatial positions of the vortex cones.

horizontal plane. The exemplary results of this experiment are presented in Fig. 7. Figure 7(a) shows the same phase profile shown in Fig. 4, which serves as a reference for comparison, through which four vortex cones are arranged on four vertices of a square.

The phase profiles obtained by superposing the blazed linear phase profile, which varies $16\pi$ (rad) from one end to the other end of the aperture, and the reference phase profile, shown in Figs. 7(b) and 7(c), make the corresponding vortex cones shift horizontally without degrading the shape. In Figs. 7(e) and 7(h), the vortex cone on the third quadrant is shifted downward without having an effect on the other vortex cones. The second example in Fig. 7(c) produces multiple vortex cones with the vortex cone on the first quadrant tilted upward and that on the third quadrant tilted downward.

Slightly separated and independently controlled multiple vortex cones were experimentally generated and measured. Through the experiments, we confirmed that the direct-phase modulation technique is effective for controlling the topological charges and relative horizontal positions of tiny free-space vortex cones dynamically.

## 4. Conclusion

In this paper, it has been shown that the topological charges and horizontal positions of tiny vortex cones can be successfully managed with an annular aperture array and a phase-type SLM. We have discussed the necessity of the annular aperture by contrasting the functional difference from the conventional circular aperture and tested a direct-phase modulation technique with accurate alignment to control multiple vortex cones simultaneously in free space. The proposed method addresses the technical need for dynamic control of the microscale optical field as required for various applications, such as optical tweezers, optical interconnections, and plasmonic field synthesis.

The authors acknowledge the support of the National Research Foundation and the Ministry of Education, Science and Technology of Korea through the Creative Research Initiative Program (Active Plasmonics Application Systems).

## References


1. Z. Jiang, Q. Lu, and Z. Liu, "Propagation of apertured Bessel beams," Appl. Opt. **34**, 7183–7185 (1995).
2. M. W. Beijersbergen, R. P. C. Coerwinkel, M. Kristensen, and J. P. Woerdman, "Helical-wavefront laser beams produced with a spiral phaseplate," Opt. Commun. **112**, 321–327 (1994).
3. Z. Bouchal, "Vortex array carried by a pseudo-nondiffracting beam," J. Opt. Soc. Am. A **21**, 1694–1702 (2004).
4. J. Courtial, R. Zambrini, M. R. Dennis, and M. Vasnetsov, "Angular momentum of optical vortex arrays," Opt. Express **14**, 938–949 (2006).
5. Z. Bouchal, J. Wagner, and M. Chlup, "Self-reconstruction of a distorted nondiffracting beam," Opt. Commun. **151**, 207–211 (1998).
6. C.-Y. Hwang, D. Choi, K.-Y. Kim, and B. Lee, "Dual Airy beam," Opt. Express **18**, 23504–23516 (2010).
7. H. J. Lezec, A. Degiron, E. Devaux, R. A. Linke, L. Martin-Moreno, F. J. Garcia-Vidal, and T. W. Ebbesen, "Beaming light from a subwavelength aperture," Science **297**, 820–822 (2002).
8. S. Kim, Y. Lim, H. Kim, J. Park, and B. Lee, "Optical beam focusing by a single subwavelength metal slit surrounded by chirped dielectric surface gratings," Appl. Phys. Lett. **92**, 013103 (2008).
9. H. He, M. Friese, N. Heckenberg, and H. Rubinsztein-Dunlop, "Direct observation of transfer of angular momentum to absorptive particles from a laser beam with a phase singularity," Phys. Rev. Lett. **75**, 826–829 (1995).
10. A. T. O'Neil, I. MacVicar, L. Allen, and M. J. Padgett, "Intrinsic and extrinsic nature of the orbital angular momentum of a light beam," Phys. Rev. Lett. **88**, 053601 (2002).
11. J. E. Curtis and D. G. Grier, "Modulated optical vortices," Opt. Lett. **28**, 872–874 (2003).
12. J. Curtis and D. Grier, "Structure of optical vortices," Phys. Rev. Lett. **90**, 133901 (2003).
13. C.-S. Guo, Y.-N. Yu, and Z. Hong, "Optical sorting using an array of optical vortices with fractional topological charge," Opt. Commun. **283**, 1889–1893 (2010).
14. H. Kim, J. Cho, J. Park, S. Han, and S. Seo, "Generation of mid-field concentrated beam arrays using periodic metal annular apertures," Appl. Opt. **51**, 1076–1085 (2012).
15. C.-S. Guo, X. Liu, J.-L. He, and H.-T. Wang, "Optimal annulus structures of optical vortices," Opt. Express **12**, 4625–4634 (2004).
16. T. Cizmar and K. Dholakia, "Tunable Bessel light modes: engineering the axial propagation," Opt. Express **17**, 15558–15570 (2009).
17. W. M. Lee, X. C. Yuan, and W. C. Cheong, "Optical vortex beam shaping by use of highly efficient irregular spiral phase plates for optical micromanipulation," Opt. Lett. **29**, 1796–1798 (2004).
18. Y. Izdebskaya, V. Shvedov, and A. Volyar, "Generation of higher-order optical vortices by a dielectric wedge," Opt. Lett. **30**, 2472–2474 (2005).
19. J. E. Morris, T. Cizmar, H. I. C. Dalgarno, R. F. Marchington, F. J. Gunn-Moore, and K. Dholakia, "Realization of curved Bessel beams: propagation around obstructions," J. Opt. **12**, 124002 (2010).
20. V. V. Kotlyar, A. A. Almazov, S. N. Khonina, and V. A. Soifer, "Generation of phase singularity through diffracting a plane or Gaussian beam by a spiral phase plate," J. Opt. Soc. Am. A **22**, 849–861 (2005).
21. J. Goodman, *Introduction to Fourier Optics*, 3rd ed. (Roberts and Company, 2004).